

CrystEngComm

Accepted Manuscript



This is an *Accepted Manuscript*, which has been through the Royal Society of Chemistry peer review process and has been accepted for publication.

Accepted Manuscripts are published online shortly after acceptance, before technical editing, formatting and proof reading. Using this free service, authors can make their results available to the community, in citable form, before we publish the edited article. We will replace this *Accepted Manuscript* with the edited and formatted *Advance Article* as soon as it is available.

You can find more information about *Accepted Manuscripts* in the [Information for Authors](#).

Please note that technical editing may introduce minor changes to the text and/or graphics, which may alter content. The journal's standard [Terms & Conditions](#) and the [Ethical guidelines](#) still apply. In no event shall the Royal Society of Chemistry be held responsible for any errors or omissions in this *Accepted Manuscript* or any consequences arising from the use of any information it contains.

A model for determination of the interfacial energy
from the induction time or metastable zone width data
based on turbidity measurements

Lie-Ding Shiau*, Tsan-Sheng Lu

Department of Chemical and Materials Engineering

Chang Gung University

Taoyuan 33302

Taiwan, R.O.C.

(TEL) 011-886-3-2118800 EXT. 5291

(FAX) 011-886-3-2118700

(E-mail) shiau@mail.cgu.edu.tw

*Author to whom correspondence should be addressed.

Abstract

A model is developed based on turbidity measurements of the nucleation event to correlate the classical nucleation theory with the induction time and the metastable zone width (MSZW) data, respectively. The induction time or the MSZW limit is assumed to correspond to a point at which the total projected area density of accumulated crystals along the detector direction has reached a fixed (but unknown) value, f_A . By fitting the experimental induction time data with the model, the interfacial energy of L-glutamic acid is recovered for the system by mixing aqueous sodium glutamate solution and sulfuric acid solution. Similarly, by fitting the experimental MSZW data with the model, the interfacial energy of L-glutamic acid is also recovered for cooling the aqueous L-glutamic acid solution at constant cooling rates. The results indicate that the effect of the minimum detectable size on the recovered interfacial energy is nearly negligible. The unique feature of this model is that, although f_A is unknown, the interfacial energy can

still be recovered from the induction time or the MSZW data, respectively. However, the kinetic parameter of nucleation rate can only be determined if the actual value of f_A is available.

Keywords: crystallization; nucleation; transport processes;
metastable zone width; interfacial energy

1. Introduction

Solute molecules in the supersaturated solution can aggregate and form clusters. Clusters can further aggregate to a bigger size. When the size of a cluster exceeds a critical size, it becomes thermodynamically stable and the subsequent growth leads to a new nucleus.¹⁻² Nevertheless, it is not possible to directly detect critical nuclei formation. These nuclei can only be experimentally detected after they have grown to a detectable size. Various detection techniques have been developed for experimental determination of the nucleation event, including the change of electrical conductivity,³ ultrasound velocity,⁴⁻⁷ turbidity,^{4,8-10} or video imaging¹¹ of the solution. Among these techniques, turbidity measurement has been most commonly used in recent years.

The interfacial energy of a crystalline solid in solution is a quantity of considerable importance in nucleation. In the classical nucleation theory (CNT), the

nucleation rate is expressed in the thermally activated Arrhenius form, in which temperature, supersaturation and interfacial energy govern the rate of nucleation.^{1,2}

Generally, the higher the value of interfacial energy the more difficult it is for the solute to crystallize. Due to the strong evidence of stable prenucleation clusters¹² and the differences between experimental nucleation rates and theoretical predictions by CNT, various non-classical nucleation models have been proposed in recent years.¹³⁻¹⁸ However, CNT still represents the main framework for the understanding of nucleation phenomena and is still widely adopted to describe nucleation rates for supersaturated solutions.¹⁹⁻²⁵

The induction period is defined as the time interval between the creation of the supersaturation and the formation of critical nuclei.^{1,2} Thus, the induction period is closely related to the nucleation rate in supersaturated solutions and has been frequently used as a measure of the

nucleation event to recover the interfacial energy of the crystallized substance in the literature.¹⁹⁻²⁵ Recently, Jiang and ter Horst²⁶ has developed a novel method in which nucleation rates are determined from cumulative probability distributions of induction times in agitated solutions.

Metastable zone width (MSZW) is also an important characteristic property of the crystallized substance in supersaturated solutions. MSZW is usually determined by the polythermal method when the solution is continuously cooled at a constant cooling rate.^{1,2} Although the induction period and the MSZW of a crystallization system is closely related, only a limited number of studies have been reported to recover the interfacial energy directly from the MSZW data.^{10,27}

Experimental studies of various crystallization systems have shown that the MSZW generally increases with an increase in cooling rate.³⁻¹¹ Nyvlt's approach^{28,29} has been

traditionally adopted to interpret the MSZW at constant cooling rates by the polythermal method. Recently, Sangwal³⁰ proposed the self-consistent Nyvlt-like equation using the theory of regular solutions for the temperature dependence of solubility. Based on the power-law form of the nucleation rate, these models lead to a linear relationship of $\log(\Delta T_m/T_0)$ versus $\log R$ for the experimental data on the maximum supercooling ΔT_m for solutions saturated at a temperature T_0 as a function of cooling rate R . Sangwal³¹ also developed a new approach based on CNT to analyze the MSZW determined by the polythermal method. The resulting equation yields a linear relationship of $(T_0/\Delta T_m)^2$ versus $\log R$.

Kashchiev et al.²⁷ verified based on progressive nucleation that the often used semi-empirical Nyvlt equation is an approximation which contains only the linear terms in the relationship between $\log(\Delta T_m/T_0)$ and $\log R$. The MSZW limit is assumed to correspond to a point at which the

detectable crystallite volume fraction has reached a fixed value (but unknown), f_v . Kashchiev et al.³² also developed a more simplified model for instantaneous nucleation, which also yields a linear relationship between $\log(\Delta T_m/T_0)$ and $\log R$. Recently, Camacho Corzo et al.¹⁰ applied the approach developed by Kashchiev et al.^{27,32} to assess the nucleation kinetics of methyl stearate crystallized from kerosene solutions for the dependence of the critical undercooling on the cooling rate.

As MSZW of a system depends on the detection method of the first nucleation event, Kubota³³ proposed a model based on progressive nucleation to account for the MSZW limit corresponding to a point at which the number density of accumulated crystals has reached a fixed (but unknown) value, f_N , during the cooling process. The simple power-law form of the nucleation rate is adopted in the Kubota's model,³³⁻³⁵ leading to a linear relationship of $\log \Delta T_m$ versus $\log R$.

In this work, a model is firstly developed to correlate CNT with the induction period based on turbidity measurements of the nucleation event. Secondly, the model is extended to correlate CNT with the MSZW. The model is then applied to recover the interfacial energy of L-glutamic acid from the experimental induction period data and the MSZW data, respectively.

2. Theory

When the induction time data or the MSZW data are measured by a turbidity meter, the measurements are based on the intensity change of the transmitted light along the detector direction,^{4,8-10} which is related to f_A as the intensity decrease of the transmitted light is proportional to f_A . Note that f_A depends on the measurement device and on the substance. Recently, Parisi and Chianese^{36,37} have shown that the nephelometric signal is directly

proportional to the overall surface of the suspended solid for investigation of nucleation kinetics.

Based on the classical nucleation theory,^{1,2} the nucleation rate is expressed as

$$J = A_J \exp\left[-\frac{16\pi v^2 \gamma^3}{3k_B^3 T^3 (\ln S)^2}\right] \quad (1)$$

where the molecular volume of the solute is defined as

$$v = \frac{M_w}{\rho_C N_A} \quad \text{and supersaturation ratio is defined as } S = \frac{C}{C_{eq}}.$$

A model is derived in this work for progressive nucleation to determine interfacial energy from the induction time and MSZW data, respectively. In progressive nucleation, new crystallites are continuously nucleated among the already growing ones. In the derivation, it is assumed that: (1) detection of the nucleation event is based on f_A ; (2) nuclei are born with a near-zero size; (3) the minimum detectable size for the detector is L_d . Similarly,

detection of the nucleation event based on f_V or f_N is developed in Appendix A and Appendix B, respectively.

2.1. Model for the induction time

During the induction time study, the growth time for newly born nuclei with a near-zero size grown to L_d is given by

$$\Delta t_d = \frac{L_d}{G} \quad (2)$$

where G remains constant as S and T is kept unchanged during the induction time experiment. In other words, the crystals born at $t_i - \Delta t_d$ can grow to L_d at t_i . Therefore, only the crystals born during the time $0 \sim t_i - \Delta t_d$ can grow to a size greater than L_d and be detected at t_i . On the other hand, the crystals born during the time $t_i - \Delta t_d \sim t_i$ can only grow to a size smaller than L_d and subsequently cannot be detected at t_i .

For the nuclei born at time t , they can grow from t to t_i and their surface at t_i is given by

$$A(t; t_i) = k_A G^2 (t_i - t)^2 \quad (3)$$

As only the crystals born during the time $0 \sim t_i - \Delta t_d$ can grow to a size greater than L_d and be detected at t_i , the total projected area density of these crystals in the detector direction at t_i should correspond to f_A when the induction time is detected. Thus,

$$f_A = \int_0^{t_i - \Delta t_d} J \frac{1}{4} A(t; t_i) dt = \frac{J k_A G^2 (t_i^3 - \Delta t_d^3)}{12} \quad (4)$$

where the factor $\frac{1}{4}$ is incorporated to account for the projected portion of the surface. For example, the surface of a sphere with a diameter D equals πD^2 ; the projected area in the detector direction equals $\frac{1}{4} \pi D^2$. Substituting Eq. (1) into Eq. (4) and taking the logarithm of the resulting equation yields

$$\ln\left[\frac{12}{k_A G^2 (t_i^3 - \Delta t_d^3)}\right] = \ln\left(\frac{A_J}{f_A}\right) - \frac{16\pi v^2 \gamma^3}{3k_B^3 T^3 (\ln S)^2} \quad (5)$$

Thus, a plot of $\ln\left[\frac{12}{k_A G^2 (t_i^3 - \Delta t_d^3)}\right]$ versus $\frac{1}{T^3 (\ln S)^2}$ gives a straight line, the slope and intercept of which allows to determine γ and $\frac{A_J}{f_A}$, respectively.

2.2. Model for the MSZW

During the MSZW study, the time t_m at which the MSZW limit is detected depends on L_d . To study the effects of L_d on t_m , there exists a certain time, t_d , which is defined such that

$$L_d = \int_{t_d}^{t_m} G dt \quad (6)$$

where G is a function of time as S and T varies with time during the MSZW experiment. Thus, t_d can be determined for a given L_d . Note that $0 < t_d < t_m$. As crystals are born at a near-zero size, the crystals born at t_d will grow to the size L_d at t_m . Therefore, the crystals born during the time

$t=0 \sim t_d$ can grow to a size greater than L_d and be detected at t_m . On the other hand, the crystals born during the time $t=t_d \sim t_m$ can only grow to a size smaller than L_d and subsequently cannot be detected at t_m .

If the solution is cooled at a constant rate $R = -dT/dt$ during the time $t=0 \sim t_m$, Eq.(8) reduces to

$$L_d = \frac{1}{R} \int_{T_m}^{T_d} G dT \quad (7)$$

where T_m is the maximum supercooling temperature at t_m and T_d corresponds to the temperature at t_d . Note that $\Delta T_m = T_0 - T_m$ and $T_0 > T_d > T_m$ due to $0 < t_d < t_m$. Thus, T_d can be determined for a given L_d if the growth rate G is known.

For the nuclei born at time t , they can grow from t to t_m and their surface at t_m is given by

$$A(t; t_m) = k_A \left(\int_t^{t_m} G dt \right)^2 \quad (8)$$

As only the crystals born during the time $0 \sim t_d$ can grow to a size greater than L_d and be detected at t_m , the total projected area density of these crystals in the detector direction at t_m should correspond to f_A when the MSZW limit is detected. Thus,

$$f_A = \int_0^{t_d} J \frac{A(t; t_m)}{4} dt = \int_0^{t_d} J \frac{k_A}{4} \left(\int_t^{t_m} G dt \right)^2 dt \quad (9)$$

where the factor $\frac{1}{4}$ is incorporated to account for the projected portion of the surface.

As the solution is cooled at a constant rate $R = -dT/dt$ during the time $t = 0 \sim t_m$, substituting Eq.(1) into Eq.(9) yields

$$\frac{f_A}{A_J} = \frac{k_A}{4R^3} \int_{T_d}^{T_0} \exp\left[-\frac{16\pi v^2 \gamma^3}{3k_B^3 T^3 (\ln S)^2}\right] \left(\int_{T_m}^T G dT \right)^2 dT \quad (10)$$

As the influence of L_d on the measured MSZW is usually negligible,^{34,35} $T_d = T_m$ is assumed in Eq.(10) for simplicity.

Then, nonlinear least squares regression is applied in

Eq.(10) from the experimental T_m versus R data to determine two optimal values of γ and $\frac{f_A}{A_j}$ that would minimize the quantity

$$\varepsilon = \frac{1}{H} \sum_{j=1}^H (T_{m,j,\text{exp}} - T_{m,j,\text{cal}})^2 \quad (11)$$

where H is the number of experimental runs, $T_{m,j,\text{exp}}$ is the measured MSZW limit at R_j for run j , and $T_{m,j,\text{cal}}$ is the calculated MSZW limit at R_j for run j . Note that

$$(T_{m,j,\text{exp}} - T_{m,j,\text{cal}})^2 = (\Delta T_{m,j,\text{exp}} - \Delta T_{m,j,\text{cal}})^2 \text{ due to } \Delta T_{m,j,\text{exp}} = T_0 - T_{m,j,\text{exp}} \text{ and}$$

$$\Delta T_{m,j,\text{cal}} = T_0 - T_{m,j,\text{cal}} .$$

The following procedure is adopted to determine two optimal values of γ and $\frac{f_A}{A_j}$: (a) Guess two values of γ and $\frac{f_A}{A_j}$; (b) Calculate $T_{m,j,\text{cal}}$ at R_j for run j for all experimental runs by Eq.(10) ($j=1 \sim H$); (c) Calculate ε by Eq.(11). The same procedure from (a) to (c) is repeated to find two optimal values of γ and $\frac{f_A}{A_j}$ with the smallest ε .

3. Experimental

The experimental apparatus consists of a 250ml crystallizer immersed in a programmable thermostatic water bath shown in Figure 1. The crystallizer is equipped with a magnetic stirrer at a constant stirring rate 350rpm. The turbidity probe (Crystal Eyes manufactured by HEL limited) is used to detect the nucleation event during the induction time and the MSZW study.

3.1. The induction time measurements

As it is usually difficult for the studied system rapidly cooled to the desired temperature during the induction time study, the supersaturated solution is generated by mixing equimolar solutions of the glutamate ion and the hydrogen ion. The mixed solution is rapidly stirred to reduce the nonhomogeneous supersaturation during the mixing process. In each experiment, a 100ml aqueous sodium glutamate solution is loaded into the crystallizer at the desired temperature. Then a preheated

100ml aqueous sulfuric acid solution is added to form the desired supersaturation solution of L-glutamic acid for the induction time measurements. Sodium L-glutamate monohydrate (>99%, TCI), sulfuric acid (97%, SHOWA, Japan) and deionized water are used in all experiments.

3.2. The MSZW measurements

For the MSZW study, the deionized water and L-glutamic acid (>99%, Acros) are used to prepare the supersaturation solution. In each MSZW experiment, a 200ml aqueous L-glutamic acid solution with the desired supersaturation is loaded into the crystallizer. The solution is held at 3°C above the saturated temperature for 5~10min to ensure a complete dissolution at the beginning of the experiment, which is also confirmed by the turbidity measurement. Then the supersaturated solution is generated by cooling the aqueous saturated L-glutamic acid solution at constant cooling rates for the MSZW measurements.

3.3. Determination of the polymorphic forms

L-glutamic acid has two known polymorphs, the metastable granular α -form and the stable plate-like β -form. The polymorphic fraction in the crystalline phase can be measured with Raman spectroscopy.³⁸ To determine the polymorphic forms of the formed L-glutamic acid in this study, the final dried crystals are analyzed using Raman spectroscopy (P/N LSI-DP2-785 Dimension-P2 System, 785nm, manufactured by Lambda Solutions, INC.) at the end of each experiment. It is confirmed that nucleation of α -form occurs dominantly at $35^{\circ}\text{C} \sim 40^{\circ}\text{C}$ and nearly 100% α -form crystals are obtained at the end of the experiments. Then, the nucleation of β -form starts to occur and the α -form fraction gradually decreases as temperature increases. However, the influence of supersaturation ratio on the polymorphic composition is not obvious. Note that the transformation from the metastable α -form to the stable β -form does not occur

in the solid-state.³⁹ Besides, no solution-mediated polymorph transformation is observed due to the short experimental times.^{25,40}

4. Results and discussion

As the growth mechanism of small nuclei should be surface integration controlled, the growth rate of α L-glutamic acid reported by Scholl et al.⁴¹ based on the birth and spread model is adopted here. Thus,

$$G = 3.63 * 10^{-4} T \exp\left(\frac{-3.72 * 10^3}{T}\right) (S - 1)^{2/3} (\ln S)^{1/6} \exp\left(\frac{-5.42 * 10^4}{T^2 \ln S}\right) \quad (12)$$

In the calculations, spherical nuclei are assumed for L-glutamic acid with $k_A = \pi$, $k_V = \frac{\pi}{6}$, $M_w = 0.147 \text{ kg/mol}$, $\rho_C = 1460 \text{ kg/m}^3$ and $v = 1.674 * 10^{-28} \text{ m}^3$.

4.1. The induction time study

The induction time data of L-glutamic acid measured for various supersaturations at $35^\circ\text{C} \sim 62^\circ\text{C}$ are listed in Table 1. Note that the supersaturated solution is

generated by mixing aqueous sodium glutamate solution and sulfuric acid solution. Each data point represents the average for three replicate experimental runs. In Table 1, t_i decreases with increasing S at each T . Generally, t_i also decreases with increasing T for each S .

As the minimum detectable size for the detector used in the current experiments is unknown, three cases are discussed in the followings for $L_d = 0$, $L_d = 10\mu\text{m}$ and $L_d = 25\mu\text{m}$, respectively. As calculated by Eq.(2), Tables 2(a) and 2(b) list the calculated Δt_d for $L_d = 10\mu\text{m}$ and $L_d = 25\mu\text{m}$, respectively. Note that for $L_d > 28\mu\text{m}$ some induction time data give rise to the unreasonable results of $\Delta t_d > t_i$ from Eq.(2). Figure 2(a)~2(c) show the plots of $\ln\left[\frac{12}{k_A G^2 (t_i^3 - \Delta t_d^3)}\right]$ versus $\frac{1}{T^3 (\ln S)^2}$ for all the induction time data measured at $35^\circ\text{C} \sim 62^\circ\text{C}$ with $L_d = 0$, $L_d = 10\mu\text{m}$ and $L_d = 25\mu\text{m}$, respectively.

Table 3 lists the obtained results from the linear regression plots. The obtained γ is only slightly

increases with increasing L_d and falls within the range $8.03 \sim 8.23 \text{ mJ/m}^2$, which is close to $\gamma = 9.57 \sim 10.4 \text{ mJ/m}^2$ reported by Lindenberg and Mazzotti²⁵ for the system by mixing aqueous sodium glutamate solution and hydrochloric acid solution. Note that hydrochloric acid is replaced by sulfuric acid in this work.

Mersmann⁴² correlated the interfacial energy with the solubility of the compound as

$$\gamma = \beta kT \frac{1}{v^{2/3}} \ln \frac{\rho_C}{C_{eq}(T)} \quad (13)$$

where $\beta = 0.514$ for spherical nuclei.⁴³ Eq. (13) predicts $\gamma = 29.6 \sim 34.4 \text{ mJ/m}^2$ at $35^\circ\text{C} \sim 62^\circ\text{C}$. Deij et al.⁴⁴ reported $\gamma = 26.5 \text{ mJ/m}^2$ at 27°C for homogeneous nucleation of L-glutamic acid by Monte Carlo simulations. As γ obtained in this work is much lower than that predicted for homogeneous nucleation by Mersmann⁴² or Deij et al.,⁴⁴ it indicates a heterogeneous nucleation mechanism as similar to the study reported by Lindenberg and Mazzotti.²⁵

In Table 3, the recovered $\frac{A_j}{f_A}$ increases with increasing L_d . The kinetic parameter A_j can be determined if the actual value of f_A is available. Based on the study for 28 inorganic systems, Mersmann and Bartosch⁴⁵ estimated $f_V = 10^{-4} \sim 10^{-3}$ with a corresponding minimum detectable size of $10 \sim 100 \mu\text{m}$. Thus, it is assumed $f_V = 4 * 10^{-4}$ for L-glutamic acid in this work. For simplicity, spherical nuclei are assumed with $L_d = 10 \mu\text{m}$, leading to $f_N = 7.64 * 10^{11} \text{ m}^{-3}$ and $f_A = 2.40 * 10^2 \text{ m}^{-1}$. As listed in Table 3, A_j falls in the range $1.1 * 10^{11} \sim 1.8 * 10^{11} \text{ m}^{-3} \text{ s}^{-1}$.

4.2. The MSZW study

The MSZW data of the aqueous saturated L-glutamic acid solution measured for $35^{\circ}\text{C} \sim 55^{\circ}\text{C}$ at various cooling rates are listed in Table 4. Note that the supersaturated solution is generated by cooling the aqueous saturated L-glutamic acid solution at constant cooling rates. Each data point represents the average for three replicate

experimental runs. In Table 4, ΔT_m increases with increasing R for each T while ΔT_m decreases with increasing T for each R .

Figures 3(a)~3(b) illustrate the variations of T , S , G and $\frac{J}{A_j}$ with increasing time during the cooling process for the experimental run of $T_0=40^{\circ}C$, $C_0=15.1 \text{ g/kg water}$ and $T_m=23^{\circ}C$ at $R=2.5*10^{-3}K/s$. In Figure 3(a), as the solution is cooled at a constant rate, we can derive $T=T_0-Rt$, leading to $t_m=6800 \text{ s}$. As C_0 is assumed unchanged during the cooling process, S is given by $\frac{C_0}{C_{eq}}$, where C_{eq} is a function of T . In Figure 3(b), Eq.(12) is used to calculate G and Eq.(1) is used to calculate $\frac{J}{A_j}$ by assuming $\gamma=3.5 \text{ mJ/m}^2$. Relative nucleation rate can be compared from the variations of $\frac{J}{A_j}$ with increasing time although A_j is unknown.

As calculated by Eq.(7), Table 5 lists the calculated T_d for $L_d=25\mu\text{m}$. Thus, it is reasonable to assume $T_d=T_m$

for $L_d \leq 25 \mu\text{m}$ in Eq.(10). Table 6 lists the fitted results from the nonlinear regression of Eq.(10). Figure 4 shows the measured ΔT_m versus R data for $T_0 = 35^\circ\text{C} \sim 55^\circ\text{C}$; lines are the fitted results using the optimal values of γ and $\frac{f_A}{A_J}$ in Table 6. For example, the five data points of ΔT_m versus R at $T_0 = 35^\circ\text{C}$ are used to recover the optimal values of γ and $\frac{f_A}{A_J}$, leading to $\gamma = 4.1 \text{ mJ/m}^2$, $\frac{f_A}{A_J} = 3.0 \cdot 10^{-5} \text{ m}^2\text{s}$ and $\varepsilon = 1.048 \text{ K}^2$. Similarly, spherical nuclei are assumed with $f_V = 4 \cdot 10^{-4}$ and $L_d = 10 \mu\text{m}$, leading to $f_N = 7.64 \cdot 10^{11} \text{ m}^{-3}$ and $f_A = 2.40 \cdot 10^2 \text{ m}^{-1}$. As listed in Table 6, A_J falls in the range $1.2 \cdot 10^6 \sim 3.0 \cdot 10^7 \text{ m}^{-3}\text{s}^{-1}$.

As shown in Figure 4, the measured ΔT_m versus R data for $T_0 = 35^\circ\text{C} \sim 55^\circ\text{C}$ are fitted well by the present model. Table 6 indicates that γ decreases with increasing temperature and falls within the range $0.6 \sim 4.1 \text{ mJ/m}^2$, which also indicates a heterogeneous nucleation mechanism as compared to γ predicted for homogeneous nucleation by Mersmann⁴² or Deij et al.⁴⁴ Thus, γ recovered from the MSZW

study by cooling the aqueous saturated L-glutamic acid solution is smaller than that obtained from the induction time study by mixing aqueous sodium glutamate solution and sulfuric acid solution. As a greater interfacial energy implies more difficult nucleation, the existence of sodium and sulfate ions during the induction time study might hinder the binding between glutamate and hydrogen ions during the nucleation of L-glutamic acid and subsequently leads to a greater interfacial energy.

4. Conclusions

A model is developed based on turbidity measurements of the nucleation event to correlate the classical nucleation theory with the induction time and the MSZW data, respectively. The induction time or MSZW limit is assumed to correspond to a point at which the total projected area density of accumulated crystals in the detector direction has reached a fixed (but unknown) value.

This model is applied to recover γ from the induction time study by mixing aqueous sodium glutamate solution and sulfuric acid solution for $35^{\circ}\text{C} \sim 62^{\circ}\text{C}$, leading to $\gamma = 8.03 \sim 8.23 \text{ mJ/m}^2$. The results indicate that the effect of the minimum detectable size on γ is nearly negligible. The model is also applied to recover γ from the MSZW study by cooling the aqueous saturated L-glutamic acid solution at constant cooling rates for $35^{\circ}\text{C} \sim 55^{\circ}\text{C}$, leading to $\gamma = 0.6 \sim 4.1 \text{ mJ/m}^2$. As the existence of sodium and sulfate ions might hinder the binding between glutamate and hydrogen ions during the nucleation of L-glutamic acid, γ obtained from the induction time study is greater than that obtained from the MSZW study. However, both studies indicate that the nucleation mechanism is heterogeneous.

The induction time or the MSZW limit is assumed related to the total projected area density of accumulated crystals based on turbidity measurements in this work. In reality the detection limit on essentially all instruments will not

only relate to one factor (volume fraction, projected area fraction, or number density of accumulated crystals) but will be some complex functions of two or all of these factors. Therefore, this model only gives an approximation to γ even though the turbidity measurements are believed more related to the total projected area density of accumulated crystals than to the volume fraction or number density of accumulated crystals.

The growth rate of L-glutamic acid reported by Scholl et al.⁴¹ is adopted in application of the developed model. Although the growth rate of a nucleus during nucleation might be size-dependent and different from that of a microcrystal,^{1,2} this model still provides insight to recover interfacial energy of the crystallizing substance based on turbidity measurements of the nucleation event. The unique feature of this model is that, although f_A is unknown, the interfacial energy can still be recovered from the induction time or the MSZW data, respectively. However,

the kinetic parameter of nucleation rate can only be determined if the actual value of f_A is available.

Acknowledgments

The authors would like to thank Chang Gung Memorial Hospital and National Science Council of Taiwan for financial support of this research. The authors also express their gratitude to Hsiao-Han Huang, Hsiu-Yin Chiu, Kai-Liang Wang and Yu-Chau Hung for their experimental work.

Appendix A. Detection of the nucleation event based on f_V

The nucleation event is assumed to correspond to a point at which the total volume density of accumulated crystals has reached a fixed (but unknown) value, f_V .²²⁻²⁵ For example, some induction time or MSZW data are measured by a conductivity meter,³ an ultrasound sensor,⁴⁻⁷ or a densitometer⁴ for the change of solution concentration, which is related to f_V as the decrease of solution concentration is proportional to f_V . Note that f_V depends on the measurement device and on the substance.

The induction time study. For the nuclei born at time t , they can grow from t to t_i and their volume at t_i is given by

$$V(t; t_i) = k_V G^3 (t_i - t)^3 \quad (14)$$

As only the crystals born during the time $0 \sim t_i - \Delta t_d$ can grow to a size greater than L_d and be detected at t_i , the total

volume fraction of these crystals at t_i should correspond to f_V when the induction time is detected. Thus,

$$f_V = \int_0^{t_i - \Delta t_d} J V(t; t_i) dt = \frac{J k_V G^3 (t_i^4 - \Delta t_d^4)}{4} \quad (15)$$

Which reduces to the expression derived by Kashchiev et al.²² for $\Delta t_d = 0$. Substituting Eq.(1) into Eq.(15) and taking the logarithm of the resulting equation yields

$$\ln\left[\frac{4}{k_V G^3 (t_i^4 - \Delta t_d^4)}\right] = \ln\left(\frac{A_J}{f_V}\right) - \frac{16\pi v^2 \gamma^3}{3k_B^3 T^3 (\ln S)^2} \quad (16)$$

Thus, a plot of $\ln\left[\frac{4}{k_V G^3 (t_i^4 - \Delta t_d^4)}\right]$ versus $\frac{1}{T^3 (\ln S)^2}$ gives a straight line, the slope and intercept of which allows to determine γ and $\frac{A_J}{f_V}$, respectively.

The MSZW study. For the nuclei born at time t , they can grow from t to t_m and their volume at t_m is given by

$$V(t; t_m) = k_V \left(\int_t^{t_m} G dt \right)^3 \quad (17)$$

As only the crystals born during the time $0 \sim t_d$ can grow to a size greater than L_d and be detected at t_m , the total volume density of these crystals at t_m should correspond to f_V when the MSZW limit is detected. Thus,

$$f_V = \int_0^{t_d} J V(t; t_m) dt = \int_0^{t_d} J k_V \left(\int_t^{t_m} G dt \right)^3 dt \quad (18)$$

As the solution is cooled at a constant rate $R = -dT/dt$ during the time $t = 0 \sim t_m$, substituting Eq. (1) into Eq. (18) yields

$$\frac{f_V}{A_J} = \frac{k_V}{R^4} \int_{T_d}^{T_0} \exp\left[-\frac{16\pi v^2 \gamma^3}{3k_B^3 T^3 (\ln S)^2}\right] \left(\int_{T_m}^T G dT \right)^3 dT \quad (19)$$

As similar to Eq. (10), two optimal values of γ and $\frac{f_V}{A_J}$ can be determined from the experimental T_m versus R data if G is a known function of T and S .

Appendix B. Detection of the nucleation event based on f_N

For the simplest case, the nucleation event is assumed to correspond to a point at which the total number density

of accumulated crystals has reached a fixed (but unknown) value, f_N .³³⁻³⁵ For example, some induction time or MSZW data are measured by a particle counter for the change of particle number density,⁴⁷⁻⁴⁹ which is related to f_N . Note that f_N depends on the measurement device and on the substance.

The induction time study. As only the crystals born during the time $0 \sim t_i - \Delta t_d$ can grow to a size greater than L_d and be detected at t_i , the total number density of these crystals at t_i should correspond to f_N when the induction time is detected. Thus,

$$f_N = J(t_i - \Delta t_d) \quad (20)$$

Substituting Eq.(1) into Eq.(20) and taking the logarithm of the resulting equation yields

$$\ln\left(\frac{1}{t_i - \Delta t_d}\right) = \ln\left(\frac{A_J}{f_N}\right) - \frac{16\pi v^2 \gamma^3}{3k_B^3 T^3 (\ln S)^2} \quad (21)$$

which reduces to the common expression adopted in the literature for $\Delta t_d = 0$.^{1,50} Thus, a plot of $\ln\left(\frac{1}{t_i - \Delta t_d}\right)$ versus $\frac{1}{T^3(\ln S)^2}$ gives a straight line, the slope and intercept of which allows to determine γ and $\frac{A_J}{f_N}$, respectively.

The MSZW study. As only the crystals born during the time $0 \sim t_d$ can grow to a size greater than L_d and be detected at t_m , the total number density of these crystals at t_m should correspond to f_N when the MSZW limit is detected. Thus,

$$f_N = \int_0^{t_d} J dt \quad (22)$$

As the solution is cooled at a constant rate $R = -dT/dt$ during the time $t = 0 \sim t_m$, substituting Eq.(1) into Eq.(22) yields

$$\frac{f_N}{A_J} = \frac{1}{R} \int_{T_d}^{T_0} \exp\left[-\frac{16\pi v^2 \gamma^3}{3k_B^3 T^3 (\ln S)^2}\right] dT \quad (23)$$

which reduces to the expression developed by Shiau and Lu for $T_d = T_m$ (i.e. $L_d = 0$).⁵¹ As similar to Eq.(10), two optimal values of γ and $\frac{f_N}{A_j}$ can be determined from the experimental T_m versus R data.

Notation

A_j = the kinetic parameter in the nucleation rate ($m^{-3}s^{-1}$)

C = concentration of solutes (kg/m^3)

C_0 = initial saturated concentration of solutes at T_0
(kg/m^3)

C_{eq} = saturated concentration of solutes (kg/m^3)

f_A = the minimum detectable projected area density of
accumulated crystals in the detector direction
(m^2/m^3 or m^{-1})

f_N = the minimum detectable number density of accumulated
crystals (m^{-3})

f_V = the minimum detectable volume fraction of accumulated
crystals (-)

G = growth rate (m/s)

J = nucleation rate ($m^{-3}s^{-1}$)

k_A = the area shape factor (-)

k_B = the Boltzmann constant ($=1.38*10^{-23}J/K$)

k_V = the volume shape factor (-)

L_d = the minimum detectable size (m)

M_w = the molar mass (kg/mol)

N_A = Avogadro number ($= 6.02 * 10^{23} mol^{-1}$)

R = cooling rate (K/s)

S = supersaturation ratio (-)

T = temperature (K)

T_0 = initial saturated temperature (K)

T_d = temperature at t_d (K)

T_m = temperature at the MSZW limit at t_m (K)

t = time (s)

t_d = time defined in Eq.(6) (s)

t_i = induction time (s)

t_m = time at the MSZW limit (s)

Greek letters

γ = interfacial energy (J/m^2)

ρ_c = crystal density (kg/m^3)

v = volume of the solute molecule (m^3)

ε = the deviation defined in Eq.(11) (K^2)

ΔT_m = MSZW (K)

References

- 1 J. W. Mullin, *Crystallization*, Butterworth-Heinemann, Oxford, 1993.
- 2 D. Kashchiev , *Nucleation: Basic theory with applications*, Butterworth-Heinemann, Oxford, 2000.
- 3 N. Lyczko, F. Espitalier, O. Louisnard, J. Schwartzentruber, *Chem. Eng. J.*, 2002, **86**, 233-241.
- 4 B. Marciniak, *J. Cryst. Growth*, 2002, **236**, 347-356.
- 5 S. Titiz-Sargut, J. Ulrich, *Cryst. Growth Des.*, 2002, **2**, 371-374.
- 6 H. Gurbuz, B. Ozdemir, *J. Cryst. Growth*, 2003, 252, 343-349.
- 7 W. Omar, J. Ulrich, *Cryst. Growth Des.*, 2006, **6**, 1927-1930.
- 8 X. Ni, A. Liao, *Chem. Eng. J.*, 2010, **156**, 226-233.
- 9 S. S. Kadam, H. J. M. Kramer, J. H. ter Horst, *Cryst. Growth Des.*, 2011, **11**, 1271-1277.

- 10 D. M. Camacho Corzo, A. Borissova, R. B. Hammond, D. Kashchiev, K. J. Roberts, K. Lewtas, I. More, *CrystEngComm*, 2014, **16**, 974–991.
- 11 C. J. Brown, X. W. Ni, *CrystEngComm*, 2012, **14**, 2944–2949.
- 12 D. Gebauer, A. Volkel, H. Colfen, *Science*, 2008, **322**, 1819–1822.
- 13 S. L. Girshick, C. P. Chiu, *J. Chem. Phys.*, 1990, **93**, 1273–1277.
- 14 L. Granasy, D. W. Oxtoby, *J. Chem. Phys.*, 2000, **112(5)**, 2399–2409;
- 15 L. Granasy, T. Pusztai, *J. Chem. Phys.*, 2002, **117**, 6157–6168.
- 16 P. G. Vekilov, *Nanoscale*, 2010, **2**, 2346–2357.
- 17 D. Gebauer, H. Colfen, *Nano Today*, 2011, **6**, 564–584.
- 18 D. Gebauer, M. Kellermeier, J. D. Gale, L. Bergstrom, H. Colfen, *Chem. Soc. Rev.*, 2014, **43**, 2348–2371.
- 19 O. Pino-Garcia, A. C. Rasmuson, *Cryst. Growth Des.*, 2004, **4**, 1025–1037.

- 20 A. Bernardo, C. E. Calmanovici, E. A. Miranda, *Cryst. Growth Des.*, 2004, **4**, 799-805.
- 21 A. Kuldipkumar, G. S. Kwon, G. G. Z. Zhang, *Cryst. Growth Des.*, 2007, **7**, 234-242.
- 22 D. Kashchiev, D. Verdoes, G. M. van Rosmalen, *J. Cryst. Growth*, 1991, **110(3)**, 373-380.
- 23 J. Scholl, L. Vicum, M. Muller, M. Mazzotti, *Chem. Eng. Technol.*, 2006, **29(2)**, 257-264.
- 24 J. Scholl, C. Lindenberg, L. Vicum, M. Mazzotti, J. Brozio, *Cryst. Growth Des.*, 2007, **7(9)**, 1653-1661.
- 25 C. Lindenberg, M. Mazzotti, *J. Cryst. Growth*, 2009, **311**, 1178-1184.
- 26 S. Jiang, J. H. ter Horst, *Cryst. Growth Des.*, 2011, **11**, 256-261.
- 27 D. Kashchiev, A. Borissova, R. B. Hammond, K. J. Roberts, *J. Cryst. Growth*, 2010, **312**, 698-704.
- 28 J. Nyvlt, *J. Cryst. Growth*, 1968, **3/4**, 377-383.

- 29 J. Nyvlt, O. Schnell, M. Matuchova, M. Broul, *The Kinetics of Industrial Crystallization*, Academia: Prague 1985.
- 30 K. Sangwal, *Cryst. Res. Technol.*, 2009, **44**, 231-247.
- 31 K. Sangwal, *Cryst. Growth Des.*, 2009, **9**, 942-950.
- 32 D. Kashchiev, A. Borissova, R. B. Hammond, K. J. Roberts, *J. Phys. Chem.*, 2010, **114**, 5441-5446.
- 33 N. Kubota, *J. Cryst. Growth*, 2008, **310**, 629-634.
- 34 M. Kobari, N. Kubota, I. Hirasawa, *CrystEngComm*, 2013, **15**, 1199-1209.
- 35 N. Kubota, M. Kobari, I. Hirasawa, *CrystEngComm*, 2014, **16**, 1103-1112.
- 36 M. Parisi, A. Chianese, *Chemical Engineering Transactions*, 2013, **32**, 2065-2070.
- 37 M. Parisi, A. Chianese, *Chem. Eng. Technol.*, 2013, **36(8)**, 1335-1340.
- 38 T. Ono, J. H. ter Horst, P. J. Jansens, *Cryst. Growth Des.*, 2004, **4(3)**, 465-469.
- 39 M. Kitamura, *J. Cryst. Growth*, 1989, **96**, 541-546.

- 40 J. Cornel, C. Lindenberg, M. Mazzotti, *Cryst. Growth Des.*, 2009, **9(1)**, 243-252.
- 41 J. Scholl, C. Lindenberg, L. Vicum, J. Brozio, M. Mazzotti, *Faraday Discuss.*, 2007, **136**, 247-264.
- 42 A. Mersmann, *J. Cryst. Growth*, 1990, **102(4)**, 841-847.
- 43 D. Kashchiev, G. M. van Rosmalen, *Cryst. Res. Technol.*, 2003, **38(7-8)**, 555-574.
- 44 C. P. M. Roelands, J. H. ter Horst, H. J. M. Kramer, P. J. Jansens, *Cryst. Growth Des.*, 2006, **6(6)**, 1380-1392.
- 45 A. Mersmann, K. Bartosch, *J. Cryst. Growth*, 1998, **183**, 240-250.
- 46 E. Manzurola, A. Apelblat, *J. Chem. Thermodynamics*, 2002, **34**, 1127-1136.
- 47 J. W. Mullin, S. J. Jancic, *Trans. Inst. Chem. Eng.*, 1979, 57, 188-193.
- 48 M. Fujiwara, P. S. Chow, D. L. Ma, R. D. Braatz, *Cryst. Growth Des.*, 2002, 2, 363-370.
- 49 P. Barrett, B. Glennon, *Trans. Inst. Chem. Eng. Part A*, 2002, 80, 799-805.

50 O. Sohnle, J. Garside, *Precipitation*, Butterworth-Heinemann, Oxford, 1992.

51 L. D. Shiau, T. S. Lu, *J. Cryst. Growth*, 2014 (in press)

Table 1. The measured induction time data at different temperatures for various supersaturations.

	t_i (s)						
	$S=1.83$	$S=2$	$S=2.25$	$S=2.5$	$S=3$	$S=4$	$S=5$
35 °C	1032.5	375.5	241.2	138	59.5	36.3	23.5
40 °C	993.5	330.5	166	103	72.5	32.5	20.1
45 °C	374	264	131.5	77	66	22.9	18.9
55 °C	283	165.5	80	66.5	27	19	13
62 °C	316	138	54	48	31	12.6	10.2

Table 2 (a). The calculated Δt_d by Eq. (2) for $L_d = 10\mu m$.

	$\Delta t_d (s)$						
	$S = 1.83$	$S = 2$	$S = 2.25$	$S = 2.5$	$S = 3$	$S = 4$	$S = 5$
$35\text{ }^\circ C$	49.5	37.9	28.2	22.6	16.3	10.7	8.2
$40\text{ }^\circ C$	39.0	29.9	22.4	18.0	13.0	8.6	6.6
$45\text{ }^\circ C$	31.0	23.9	17.9	14.4	10.5	6.9	5.3
$55\text{ }^\circ C$	19.9	15.5	11.7	9.4	6.9	4.6	3.5
$62\text{ }^\circ C$	14.9	11.6	8.8	7.1	5.2	3.5	2.7

Table 2 (b). The calculated Δt_d by Eq. (2) for $L_d = 25 \mu\text{m}$.

	$\Delta t_d (s)$						
	$S = 1.83$	$S = 2$	$S = 2.25$	$S = 2.5$	$S = 3$	$S = 4$	$S = 5$
35°C	123.8	94.7	70.5	56.4	40.8	26.9	20.4
40°C	97.5	74.9	56.0	44.9	32.5	21.5	16.4
45°C	77.4	59.6	44.7	36.0	26.2	17.4	13.2
55°C	49.8	38.6	29.2	23.6	17.2	11.5	8.8
62°C	37.2	29.0	22.0	17.8	13.1	8.8	6.7

Table 3. The obtained results from the linear regression plots in Figures 2 (a) ~ (c) .

	γ (mJ/m ²)	$\frac{A_j}{f_A}$ (m ⁻² s ⁻¹)	A_j (m ⁻³ s ⁻¹)	R^2 (-)
$L_d = 0$	8.03	4.6×10^8	1.1×10^{11}	0.96
$L_d = 10 \mu\text{m}$	8.04	4.8×10^8	1.2×10^{11}	0.95
$L_d = 25 \mu\text{m}$	8.23	7.4×10^8	1.8×10^{11}	0.94

Table 4. The measured MSZW data for $35^{\circ}\text{C} \sim 55^{\circ}\text{C}$ at various cooling rates.

T_0 ($^{\circ}\text{C}$)	C_0 (kg/m^3)	T_m ($^{\circ}\text{C}$)				
		$R = 8.3 \times 10^{-4}$ (K/s)	$R = 1.7 \times 10^{-3}$ (K/s)	$R = 2.5 \times 10^{-3}$ (K/s)	$R = 4.2 \times 10^{-3}$ (K/s)	$R = 5.0 \times 10^{-3}$ (K/s)
35	12.2	23.0	18.0	15.8	14.1	11.0
40	15.1	29.0	26.0	23.0	21.0	19.5
45	18.5	36.0	33.5	30.0	28.0	26.5
50	22.3	42.5	40.5	38.0	37.5	35.0
55	26.6	49.0	47.5	46.5	45.0	44.0

$$C_{eq} = 9.58654 \times 10^{-3} T^2 - 5.3778 T + 759.0671 \quad ^{46} \quad (C_{eq} \text{ in } \text{kg}/\text{m}^3 \text{ or } \text{g}/\text{kg} \text{ water, and } T \text{ in } \text{K})$$

Table 5(a). The calculated T_d by Eq. (7) for $L_d = 10\mu\text{m}$.

T_0 (°C)	T_d (°C)				
	$R = 8.3 \times 10^{-4}$ (K/s)	$R = 1.7 \times 10^{-3}$ (K/s)	$R = 2.5 \times 10^{-3}$ (K/s)	$R = 4.2 \times 10^{-3}$ (K/s)	$R = 5.0 \times 10^{-3}$ (K/s)
35	23.1	18.1	16.0	14.4	11.4
40	29.1	26.1	23.2	21.2	19.8
45	36.1	33.6	30.1	28.2	26.7
50	42.7	40.7	38.2	37.8	35.3
55	49.3	47.8	46.8	45.4	44.4

Table 5(b). The calculated T_d by Eq. (7) for $L_d = 25\mu\text{m}$.

T_0 (°C)	T_d (°C)				
	$R = 8.3 \times 10^{-4}$ (K/s)	$R = 1.7 \times 10^{-3}$ (K/s)	$R = 2.5 \times 10^{-3}$ (K/s)	$R = 4.2 \times 10^{-3}$ (K/s)	$R = 5.0 \times 10^{-3}$ (K/s)
35	23.3	18.4	16.3	14.9	12.0
40	29.2	26.3	23.4	21.6	20.2
45	36.3	33.9	30.4	28.5	27.1
50	42.9	41.0	38.5	38.2	35.6
55	49.9	48.4	47.4	46.1	45.0

Table 6. The fitted results from the nonlinear regression of Eq. (10) in Figure 4.

$T_0(^{\circ}C)$	$\gamma (mJ/m^2)$	$\frac{f_A}{A_J} (m^2s)$	$\varepsilon (K^2)$	$A_J(m^{-3}s^{-1})$
35	4.1	3.0×10^{-5}	1.048	8.0×10^6
40	3.5	4.0×10^{-5}	0.289	6.0×10^6
45	1.5	2.0×10^{-4}	0.322	1.2×10^6
50	1.3	4.0×10^{-5}	0.415	6.0×10^6
55	0.6	8.0×10^{-6}	0.010	3.0×10^7

Figure captions

Schematic diagram of the experimental apparatus: (1) 250ml crystallizer, (2) magnetic stirrer, (3) constant temperature water bath, (4) turbidity probe, (5) temperature probe, (6) computer.

Figure 2. $\ln\left[\frac{12}{k_d G^2 (t_i^3 - \Delta t_d^3)}\right]$ versus $\frac{1}{T^3 (\ln S)^2}$ for (a) $L_d = 0$; (b) $L_d = 10 \mu\text{m}$; (c) $L_d = 25 \mu\text{m}$. The solid line corresponds to the best fit linear regression and the points represent the measured induction time data for $35^\circ\text{C} \sim 62^\circ\text{C}$.

Figure 3. For the experimental run of $T_0 = 40^\circ\text{C}$, $C_0 = 15.1 \text{ g/kg water}$ and $T_m = 23^\circ\text{C}$ at $R = 2.5 * 10^{-3} \text{ K/s}$ by assuming $\gamma = 3.5 \text{ mJ/m}^2$: (a) The variations of T and S with increasing time during the cooling process; (b) The variations of G and $\frac{J}{A_j}$ with increasing time during the cooling process.

Figure 4. The measured ΔT_m versus R data. The solid lines correspond to the best fit nonlinear regression of Eq. (10) and the points represent the measured MSZW data for $35^\circ\text{C} \sim 55^\circ\text{C}$.

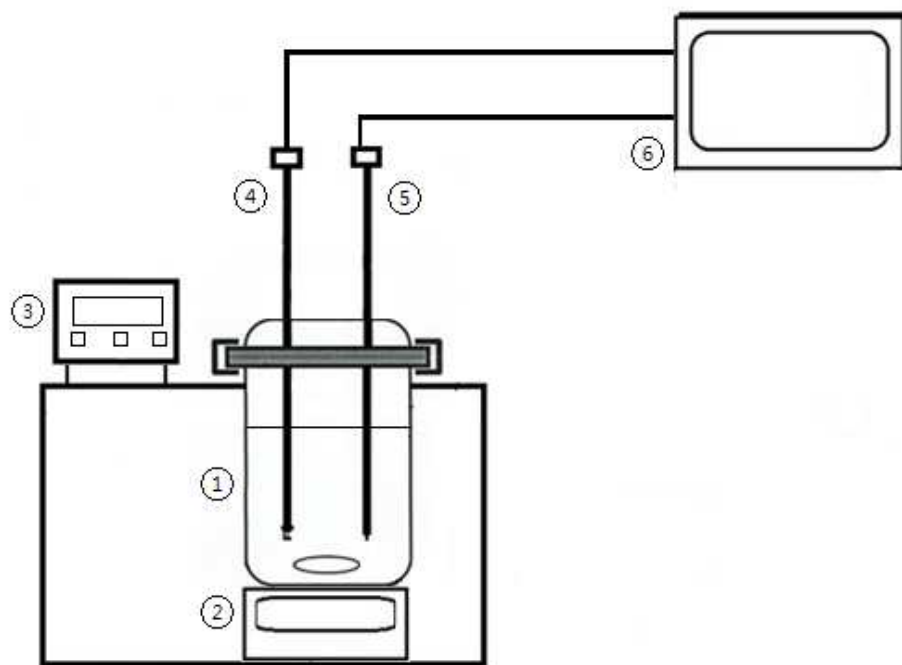


Figure 1

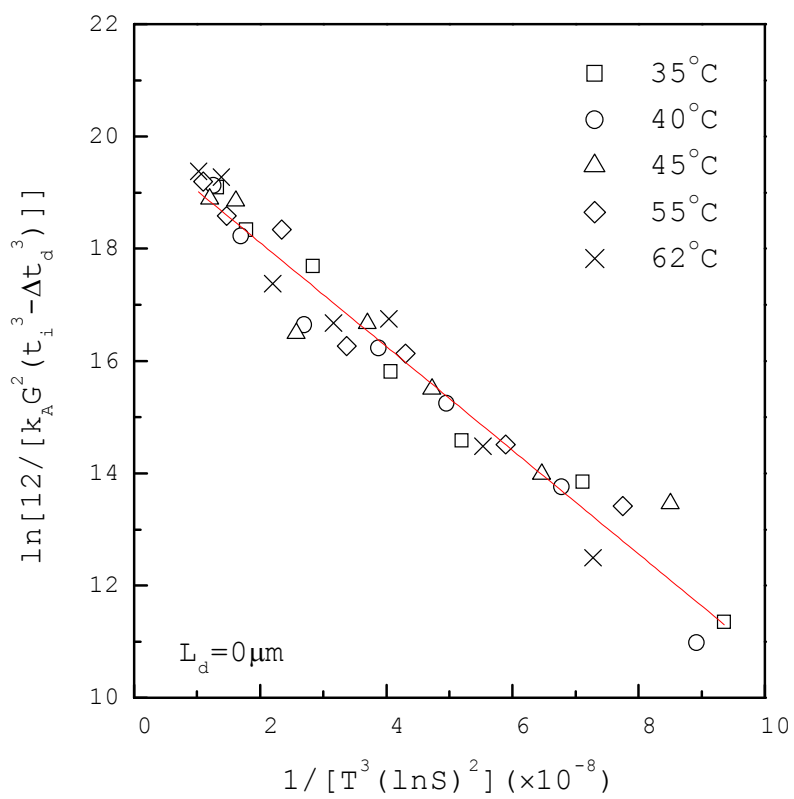


Figure 2(a)

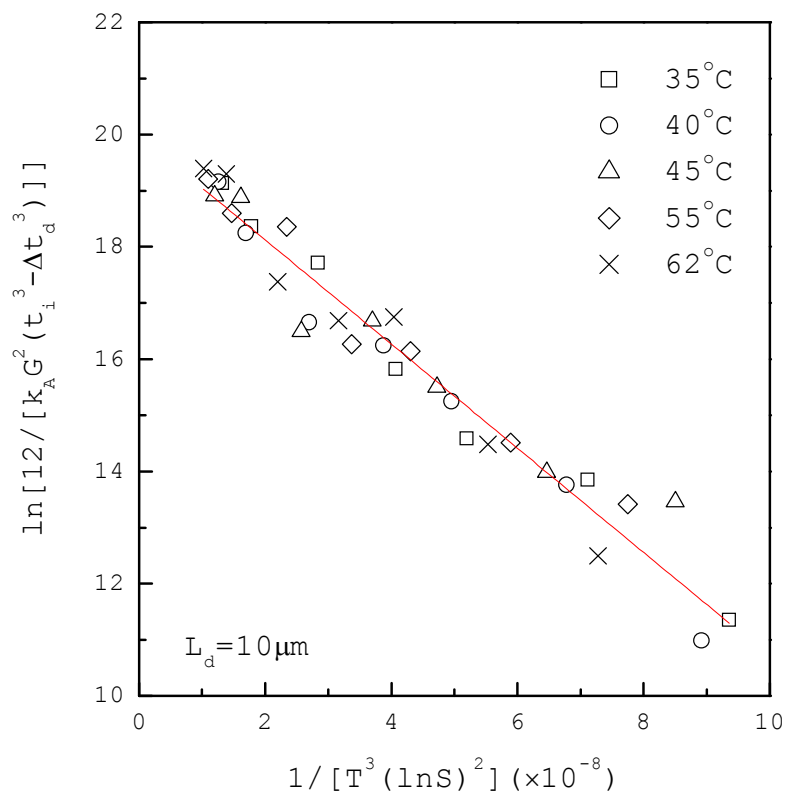


Figure 2(b)

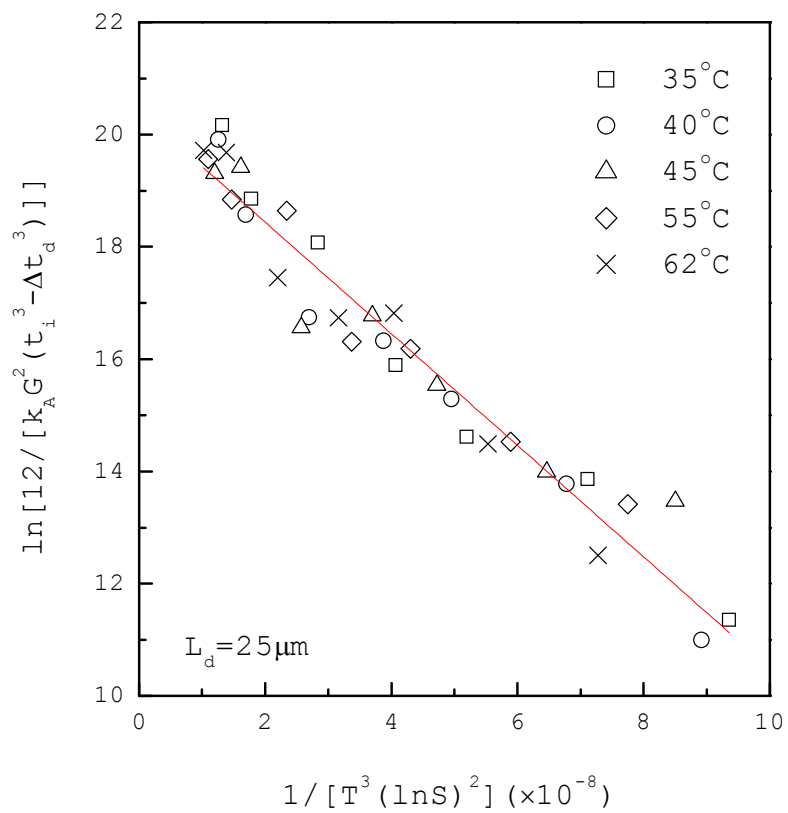


Figure 2(c)

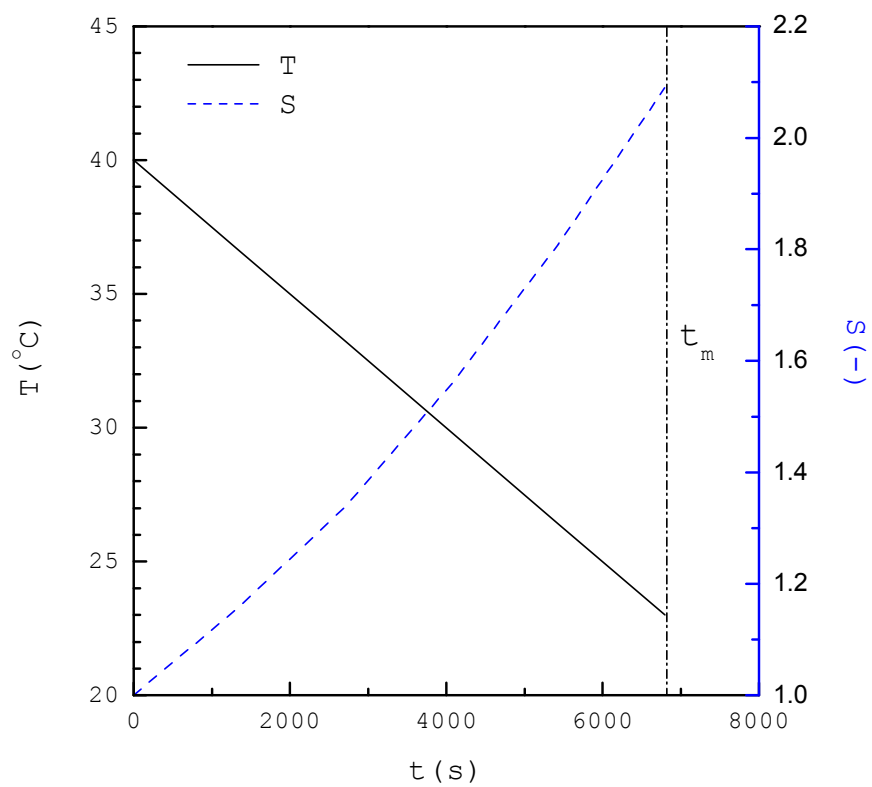


Figure 3(a)

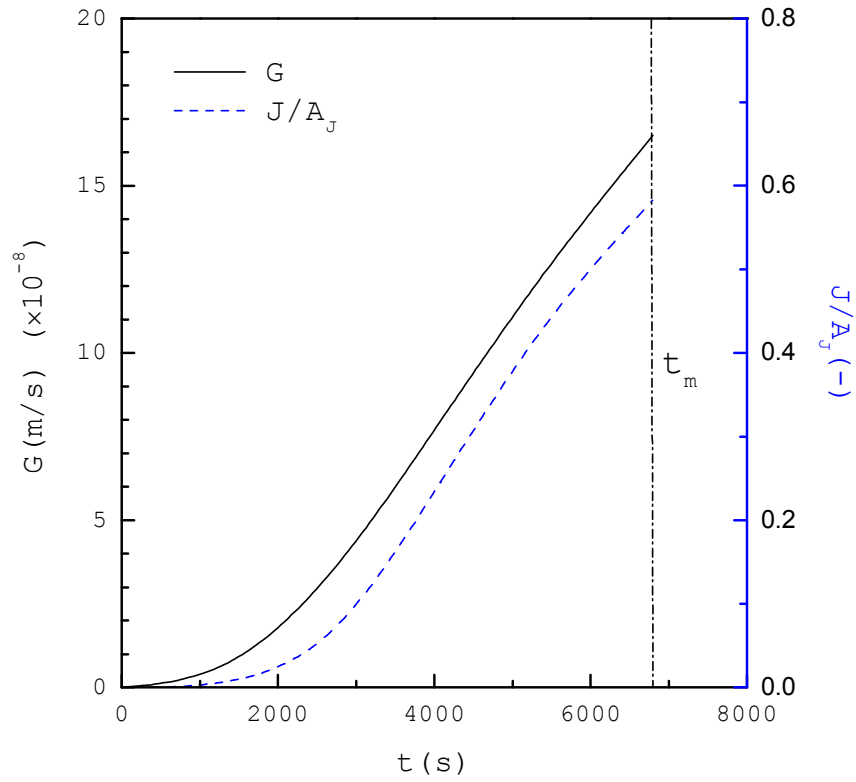


Figure 3(b)

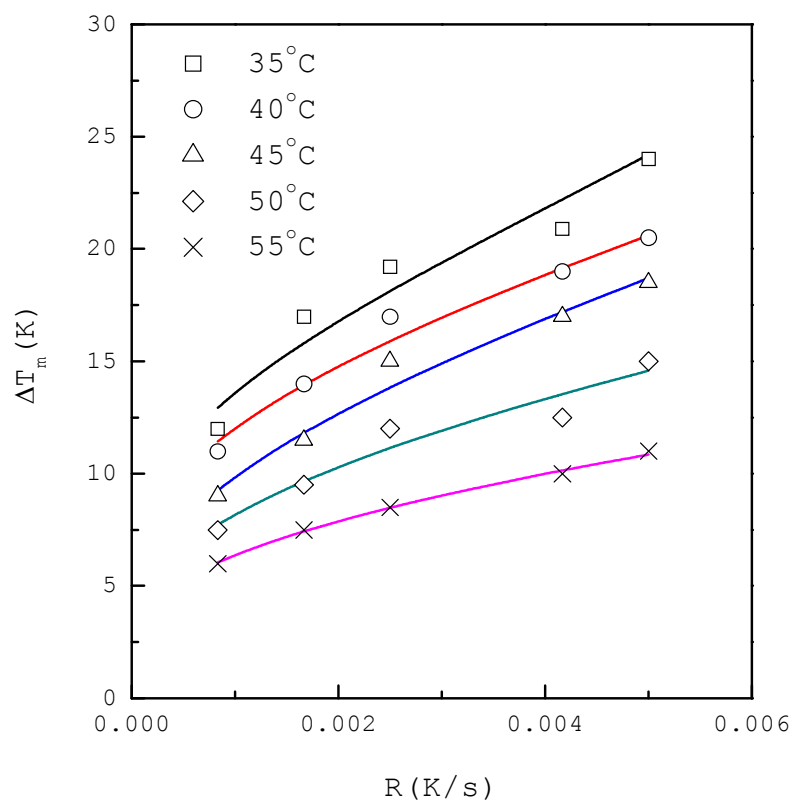
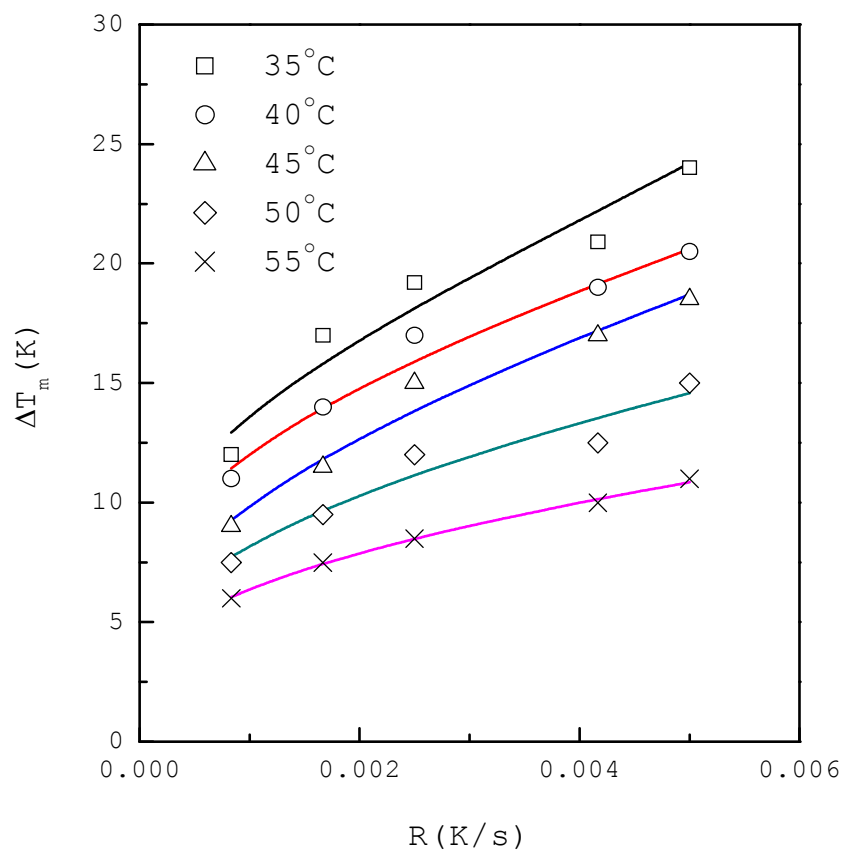


Figure 4

A model is developed to recover the interfacial energy from the induction time and the metastable zone width data, respectively.



A model is developed to recover the interfacial energy from the induction time and the metastable zone width data, respectively.